

# Quantum chemical study of the lanthanide bond length contraction on $\text{Ln}^{3+}$ -doped $\text{Cs}_2\text{NaYCl}_6$ crystals ( $\text{Ln}=\text{Ce}$ to $\text{Lu}$ )

Belén Ordejón, Luis Seijo, and Zoila Barandiarán<sup>a)</sup>

*Departamento de Química, C-XIV and Instituto Universitario de Ciencia de Materiales Nicolás Cabrera, Universidad Autónoma de Madrid, 28049 Madrid, Spain*

(Received 6 June 2003; accepted 1 July 2003)

The lanthanide–chlorine bond length,  $R_e$ , and the frequency of the symmetric stretching mode,  $\bar{\nu}_{a_{1g}}$ , of the  $(\text{LnCl}_6)^{3-}$  octahedral defect clusters embedded in  $\text{Cs}_2\text{NaYCl}_6$  have been calculated for all 14  $\text{Ce}^{3+}$  to  $\text{Lu}^{3+}$  impurities in their ground  $4f^n$  electronic state using wave-function-based *ab initio* methods of solid state quantum chemistry which include relativistic effects and electron correlation within the  $(\text{LnCl}_6)^{3-}$  defect clusters and quantum mechanical interactions between the  $(\text{LnCl}_6)^{3-}$  electronic group and the  $\text{Cs}_2\text{NaYCl}_6$  embedding host ions. The bond distance values obtained provide useful data to improve the Judd–Morrison model of the  $4f \rightarrow 5d$  energy separation by explicitly including the local distortions the  $\text{Ln}^{3+}$  ions produce in the  $\text{Cs}_2\text{NaYCl}_6$  host. The values of the structural parameters  $R_e$  and  $\bar{\nu}_{a_{1g}}$ , and their variation across the series have also been studied using simpler models of the embedding host (*in vacuo* and Madelung embeddings), which has revealed that host effects, particularly those associated with quantum mechanical interactions, strengthen the Ln–Cl bond (decreasing the bond distances and increasing the frequencies of the symmetric bond stretch) and are smaller towards the right end of the series. Electron correlation within the  $(\text{LnCl}_6)^{3-}$  clusters also reduces the bond distance values, but this reduction increases going right from Ce to Lu; its effects on the frequencies of the symmetric stretching mode are negligible. The comparison of the theoretical results with the few available experiments is very satisfactory. © 2003 American Institute of Physics. [DOI: 10.1063/1.1602692]

## I. INTRODUCTION

Very little quantitative information is available on the local geometry of lanthanide (Ln) and actinide (An) impurities in solids, in spite of the fact that their electronic transitions are known to depend on their structural parameters through large powers [typically  $-5$ ,  $-6$  powers of the Ln (An)—ligand bond lengths].<sup>1–3</sup> As a consequence of this lack of structural information and together with the fact that the band shapes depend on the square of the bond length offsets between the initial and final electronic states, but not on their sign, it has been widely accepted that the bond distances in Ln and An doped crystals are larger in the  $f^{n-1}d^1$  energy levels than in the case of the  $f^n$  configuration,<sup>4–7</sup> even when this idea has been neither confirmed nor rejected from experiments. On the contrary, it has been contradicted by a number of solid state quantum chemistry works on Ln and An ions in halide crystals<sup>8–11</sup> and has been specifically addressed and interpreted using quantum chemistry methods for the analysis of the bonding in Ref. 12.

A good example of the imbalanced spectroscopic and structural information available can be found in the series of  $\text{Ln}^{3+}$ -doped ( $\text{Ln}=\text{Ce}$  to  $\text{Lu}$ ) crystals, which have been considered interesting model systems where the  $\text{Ln}^{3+}$  ions occupy perfect octahedral sites substituting for  $\text{Y}^{3+}$  cations. Their electronic structure has been extensively studied for decades using spectroscopic techniques (some representative

works can be found in Refs. 13–19). However, no reports on direct experimental measurements of the Ln–Cl bond lengths is available, to our knowledge, even though the expected lanthanide bond length contraction across the series should have an impact on the actual local distortions of the host and on the spectroscopic properties associated with the impurities.

In this context, it has been pointed out the need for structural data in order to enforce the capabilities of predictive classical models for  $\text{Ln}^{3+}$ -doped crystals.<sup>20</sup> In effect, it has been recently concluded by Bettinelli and Moncorgé<sup>20</sup> that the model proposed by Morrison<sup>3</sup> based on Judd's suggestions<sup>2</sup> to account for the effects of induced dipole moments of polarizable ligands on the  $4f-5d$  electronic transitions of lanthanide ions in solids, is useful to interpret the general behavior of the lowest  $4f-5d$  electronic transitions of  $\text{Ln}^{3+}$  shown by Dorenbos through the compilation and analysis of experimental data of over 300  $\text{Ln}^{3+}$ -doped crystals.<sup>21,22</sup> According to the Judd–Morrison model,<sup>2,3</sup> the depression of the  $4f-5d$  transition energy of a  $\text{Ln}^{3+}$  in a crystal ( $\Delta_{fd}^0 - \Delta_{fd}$ ) relative to its value for the free ion in gas phase ( $\Delta_{fd}^0$ ), depends on two factors:  $\Delta_{fd}^0 - \Delta_{fd} = \sigma_2 S$ , defined as  $\sigma_2 = \langle r^2 \rangle_{4f^{n-1}5d} - \langle r^2 \rangle_{4f^n}$  and  $S = \sum_i \alpha_i Z_i e^2 / R_i^6$ , where  $\alpha_i$  is the polarizability of the  $i$ th ligand and  $Z_i$  is the number of ligands at a distance  $R_i$  from the metal.

Bettinelli and Moncorgé<sup>20</sup> have commented on the approximations involved in the model and its applications, such as considering that the  $R_i$  distances do not change upon doping, which makes the  $S$  factor host dependent and lanthanide

<sup>a)</sup>Author to whom correspondence should be addressed. Electronic mail: zoila.barandiaran@uam.es

independent. They have also stressed, as an important conclusion of their work, the need to refine the model in order to use it to predict the energy positions of the  $5d$  levels of  $\text{Ln}^{3+}$  ions in a wide type of materials.<sup>20</sup> In particular, they have suggested that improvements to the Judd–Morrison model could come from the inclusion of the effects on  $S$  of the actual local distortion induced by the  $\text{Ln}^{3+}$  impurity. However, this distortion could be difficult to evaluate from an experimental point of view, as it would require EXAFS measurements, which demand the use of synchrotron radiation facilities not readily available for all experimenters.<sup>20</sup>

The required lanthanide–ligand distances  $R_i$  can be obtained directly from quantum chemical calculations on the  $\text{Ln}^{3+}$  defects in a particular host crystal, as it has been recently demonstrated,<sup>8–10</sup> and, therefore, an important objective of this paper is to calculate the equilibrium geometry of the electronic ground state of the  $\text{Cs}_2\text{NaYCl}_6:(\text{LnCl}_6)^{3-}$  embedded clusters. This alternative, apart from providing the local structure parameters (i.e., bond lengths and symmetric bond stretching vibrational frequencies), and their variation across the lanthanide series, could enable an interesting combination of the Judd–Morrison model with *ab initio* embedded cluster models of quantum chemistry.<sup>23,24</sup>

In this work we have used the *ab initio* model potential (AIMP) embedded cluster method<sup>23,24</sup> to optimize the geometry of the ground state of the octahedral defects created by the  $\text{Ln}^{3+}$  ( $\text{Ce}^{3+}$  to  $\text{Lu}^{3+}$ ) impurities in the  $\text{Cs}_2\text{NaYCl}_6$  host. The calculations include electron correlation and relativistic effects within the  $(\text{LnCl}_6)^{3-}$  defect cluster and quantum mechanical interactions with the surrounding host lattice. The lanthanide bond length contraction has also been studied using the Madelung embedding and *in vacuo*, all of which serves to analyze the importance of the quantum mechanical and classical interactions between the  $(\text{LnCl}_6)^{3-}$  defect clusters and their crystalline surrounding. Experimental values of the  $\text{Ln}–\text{Cl}$  bond lengths are not available, to our knowledge;  $\bar{v}_{a_{1g}}$  experimental values on the  $\text{Cs}_2\text{NaYCl}_6:\text{Ln}^{3+}$  doped crystals are only available for  $\text{Ce}^{3+}$  and  $\text{Pr}^{3+}$ , and the comparison with our results is very good. The comparison of our  $\bar{v}_{a_{1g}}$  results with experimental data on the perfect  $\text{Cs}_2\text{NaLnCl}_6$  crystals are also presented.

## II. DETAILS OF THE CALCULATIONS

The interest of this paper is focused on the calculation of the potential energy surface of the electronic ground states of  $\text{Ln}^{3+}$ -doped  $\text{Cs}_2\text{NaYCl}_6$  ( $\text{Ln}=\text{Ce}$  to  $\text{Lu}$ ) which are localized around the  $\text{Ln}^{3+}$  impurities. These impurities substitute for some of the  $\text{Y}^{3+}$  ions in an  $O_h$  site with a first coordination shell of six  $\text{Cl}^-$  ions, whose positions become directly affected by the substitution. The local ground states depend on all the electronic interactions within  $\text{Ln}^{3+}$  and on the bonding interactions between  $\text{Ln}^{3+}$  and the six  $\text{Cl}^-$  ions, but they also depend notably on the interactions between the  $(\text{LnCl}_6)^{3-}$  cluster and the rest of the host. In consequence, a method is needed which reliably considers: (i) relativistic effects on  $\text{Ln}^{3+}$ , (ii) the major contributions of  $(\text{LnCl}_6)^{3-}$  electron correlation, and (iii) the classical and quantum embedding effects brought about by the  $\text{Cs}_2\text{NaYCl}_6$  ionic host

into the  $(\text{LnCl}_6)^{3-}$  cluster. All three contributions have been taken into account in this work by using the AIMP embedded cluster Hamiltonian, which embodies relativistic and host effects in nonparametric model potentials that are obtained directly from the operators they represent,<sup>23–25</sup> and multireference wavefunction based methods<sup>26–28</sup> that take into account electron correlation within the  $(\text{LnCl}_6)^{3-}$  unit, which have been detailed elsewhere and are referred to and summarized next.

### A. Relativistic embedded cluster Hamiltonian

The relativistic and host effects on the  $(\text{LnCl}_6)^{3-}$  electronic structure are incorporated in the calculations through the following valence only, spin-free relativistic Wood–Boring<sup>29</sup> AIMP embedded cluster Hamiltonian for the  $\text{Cs}_2\text{NaYCl}_6:(\text{LnCl}_6)^{3-}$ , which has been fully described in Refs. 9 and 24:

$$\begin{aligned} \hat{H}_{\text{spin-free}}^{\text{AIMP}} = & \sum_{i=1}^{N_{\text{val}}^{\text{clus}}} \left\{ -\frac{1}{2} \hat{\nabla}_i^2 + \sum_{\mu \in \text{clus}}^{N_{\text{nuc}}^{\text{clus}}} \left[ -\frac{Z_{\mu}^{\text{eff}}}{r_{\mu i}} + \hat{V}_{\mu\text{-core}}^{\text{AIMP}}(i) \right] \right. \\ & \left. + \sum_{\xi \in \text{host}}^{N_{\text{ion}}^{\text{host}}} \hat{V}_{\xi\text{-ion}}^{\text{emb-AIMP}}(i) \right\} + \sum_{i=1}^{N_{\text{val}}^{\text{clus}}} \sum_{j>i}^{N_{\text{val}}^{\text{clus}}} \frac{1}{r_{ij}} \\ & + \sum_{\mu \in \text{clus}}^{N_{\text{nuc}}^{\text{clus}}} \sum_{\nu(>\mu) \in \text{clus}}^{N_{\text{nuc}}^{\text{clus}}} \frac{Z_{\mu}^{\text{eff}} Z_{\nu}^{\text{eff}}}{R_{\mu\nu}}. \end{aligned} \quad (1)$$

In Eq. (1), the indices  $i$  and  $j$  refer to the  $N_{\text{val}}^{\text{clus}}$  valence electrons of the cluster,  $\mu$  and  $\nu$  refer to the  $N_{\text{nuc}}^{\text{clus}}$  nuclei (atoms) of the  $(\text{LnCl}_6)^{3-}$  cluster, each of them having  $N_{\mu}^{\text{core}}$  core electrons and an effective nuclear charge  $Z_{\mu}^{\text{eff}} = Z_{\mu} - N_{\mu}^{\text{core}}$ . The  $\xi$  index refers to the  $N_{\text{ion}}^{\text{host}}$  ions of the  $\text{Cs}_2\text{NaYCl}_6$  embedding host, i.e., all the ions in the doped material except the  $\text{Ln}^{3+}$  impurity and its first coordination shell of six  $\text{Cl}^-$  ions.

The relativistic effects are concentrated in the terms  $\hat{V}_{\mu\text{-core}}^{\text{AIMP}}(i)$  of the Hamiltonian. Each of them is the one-electron spin-free relativistic *ab initio* model potential,<sup>30</sup> which represents the effects of the core electrons of atom  $\mu$  (an effective core potential) plus the scalar Darwin and mass-velocity atomic potentials of Cowan and Griffin (which are variationally stable)<sup>31</sup> acting on the valence electrons. It reads,

$$\begin{aligned} \hat{V}_{\mu\text{-core}}^{\text{AIMP}}(i) = & \frac{1}{r_{\mu i}} \sum_k C_k^{\mu} \exp(-\alpha_k^{\mu} r_{\mu i}^2) \\ & + \sum_j \sum_k |\chi_j^{\mu}\rangle A_{j,k}^{\mu} \langle \chi_k^{\mu}| \\ & + \sum_{c \in \mu\text{-core}} D_c^{\mu} |\phi_c^{\mu}\rangle \langle \phi_c^{\mu}|. \end{aligned} \quad (2)$$

The first term on the right-hand side of Eq. (2) is the core Coulomb model potential, which is produced by least-squares fitting to the true core Coulomb potential of atom  $\mu$ .<sup>25</sup> The second term is the core exchange, plus Darwin, plus mass-velocity model potential, which is produced by the spectral representation of the true operators in the space de-

finied by the one-center basis set  $\{|\chi_j^\mu\rangle\}$ ; <sup>25</sup> this basis set is chosen to be made of all the Gaussian primitive functions used in the embedded cluster calculation that are centered on atom  $\mu$ . The third term is the core shifting operator of Huzinaga and Cantu <sup>32</sup> that prevents the valence orbitals from collapsing onto the core orbitals. It has been recently demonstrated that spin-orbit coupling does not affect structural parameters like the ones which are the goal of this work <sup>8-10</sup> and it is for this reason that spin-orbit terms have been omitted in the AIMP embedded cluster Hamiltonian.

The classical and quantum mechanical effects of the surrounding crystal are embodied in the AIMP embedding potential: the  $\xi$ -sum of  $\hat{V}_{\xi\text{-ion}}^{\text{emb-AIMP}}(i)$  terms of the Hamiltonian. Each host ion  $\xi$  contribution reads: <sup>23</sup>

$$\begin{aligned} \hat{V}_{\xi\text{-ion}}^{\text{emb-AIMP}}(i) = & -\frac{Q_\xi}{r_{\xi i}} + \frac{1}{r_{\xi i}} \sum_k C_k^\xi \exp(-\alpha_k^\xi r_{\xi i}^2) \\ & + \sum_j \sum_k |\chi_j^\xi\rangle A_{j,k}^\xi \langle \chi_k^\xi| \\ & + \sum_{c \in \xi\text{-ion}} D_c^\xi |\phi_c^\xi\rangle \langle \phi_c^\xi|. \end{aligned} \quad (3)$$

The term  $-Q_\xi/r_{\xi i}$ , represents the long-range Coulomb (Madelung) potential created by a point charge  $Q_\xi$  (the ionic charge). The next two terms of this model potential are, respectively, approximations to the short-range Coulomb potential of the full ion (which represents a correction of the point charge potential taking into account the spatial distribution of the electron charge density of the lattice ion), and to the full ion exchange operator (which stems from the fact that the generalized antisymmetric product of the cluster and the external ion wave functions must fulfill the first principles requirement of antisymmetry with respect to the interchange of electrons between cluster and host ion electronic groups). <sup>23,24</sup> The last term in Eq. (3) is the full ion projection operator, which prevents the cluster wave functions from collapsing onto this particular lattice ion. <sup>32</sup> The ingredients of the embedding potentials are obtained by performing preparatory Hartree-Fock self-consistent embedded ions calculations on  $\text{Cs}_2\text{NaYCl}_6:\text{X}$  ( $\text{X} = \text{Cs}^+$ ,  $\text{Na}^+$ ,  $\text{Y}^{3+}$ , and  $\text{Cl}^-$ ). The corresponding atomic basis sets ( $\chi_j^\xi$ ), occupied orbitals ( $\phi_c^\xi$ ) and orbital energies are used to produce the AIMP representations described above, following the AIMP recipes for representation of operators (see Refs. 23 and 24 for further details).

The actual core and embedding AIMP operators used in this work are described in the next section.

## B. The $(\text{LnCl}_6)^{3-}$ wave functions and energies: Electron correlation

In order to account for electron correlation effects on the parameters of the local structure of the  $\text{Cs}_2\text{NaYCl}_6:(\text{LnCl}_6)^{3-}$  embedded clusters, we performed complete active space self-consistent-field calculations <sup>26</sup> (CASSCF) on the  $4f^n$  high-spin electronic ground state generating all possible configurations where the  $n$  ( $n=1-14$ ) open-shell electrons occupy the 12 molecular orbitals of

main character Ln  $4f$  ( $a_{2u}$ ,  $t_{2u}$ ,  $t_{1u}$ ) and Ln  $5d$  ( $t_{2g}$ ,  $e_g$ ). (Note that we will refer to the molecular orbitals by their main atomic orbital character all throughout this paper.) These wave functions were considered to be the zeroth order for subsequent second order perturbation theory calculations (CASPT2) <sup>27,28</sup> where  $56+n$  valence electrons of the  $(\text{LnCl}_6)^{3-}$  clusters were correlated. These electrons occupy the molecular orbitals of main character Ln  $5s$ ,  $5p$ ,  $4f$ ,  $5d$  and Cl  $3s$ ,  $3p$ . The CASPT2 calculations revealed large and uniform weights ( $>60\%$ ) of the zeroth order reference in all states calculated at all distances and showed no signs of problems of intruder states, nor large contributions to the first order wavefunction nor to the second order energy correction which would indicate inadequacies on the choice of the complete active space used. Also, the CASPT2 potential energy surfaces were found to be continuous functions of the Ln-Cl distance.

All the CASSCF+CASPT2 calculations were done using the relativistic spin-free AIMP embedded cluster Hamiltonian described in the preceding section. <sup>33</sup> The core and embedding AIMP operators, and valence basis sets used in this work are the following: For the  $\text{Ln}^{3+}$  we used the  $[\text{Kr},4d]$  core spin free relativistic Cowan-Griffin-Wood-Boring AIMP and  $(14s10p9d8f)$  valence basis sets from Ref. 34. Three Gaussian functions of  $g$  type,  $3g$ , which were obtained by maximum radial overlap with the Ln  $4f$  orbitals, were used as polarization functions. The final contraction of the basis set was  $\text{Ln}[6s5p5d4d1f]$ . For chlorine, we used the  $[\text{Ne}]$  core relativistic Cowan-Griffin-Wood-Boring AIMP and valence basis set  $(7s6p)$  of Ref. 30 augmented by  $1p$  diffuse function for anions, <sup>35</sup> and  $1d$  polarization function, <sup>36</sup> the final contraction being  $[3s4p1d]$ . The  $(7s4p)$  basis set of the second neighbor  $\text{Na}^+$  ions from Ref. 37 was also included on the basis set of the  $(\text{LnCl}_6)^{3-}$  clusters, contracted as  $[1s1p]$ ; these so-called second-neighbor basis functions are needed to fulfill strong-orthogonality conditions with the lattice ion wave functions on crystals like the  $\text{Cs}_2\text{NaYCl}_6$  elpasolite where  $\text{Na}^+$  ions occur at near (100) sites. <sup>24,38</sup> The embedding potential used to describe the interactions between the  $(\text{LnCl}_6)^{3-}$  defect clusters and their  $\text{Cs}_2\text{NaYCl}_6$  crystalline environment was obtained in Ref. 37; it has been used to study the structure and spectroscopy of transition metal ion impurities at ambient and high pressures, <sup>37,39</sup> and lanthanide/actinide ion impurities. <sup>8-11</sup> The MOLCAS-5 program system <sup>40</sup> was used to compute the embedded cluster wave functions and energies.

## III. RESULTS

We calculated the embedded cluster energy of the ground state of the octahedral  $(\text{LnCl}_6)^{3-}$  clusters at a number of  $R(\text{Ln-Cl})$  distances using the methods described in Sec. II. These numerical potential energy surfaces were fitted to third-degree polynomials from which the equilibrium distances  $R_e$  and totally symmetric vibrational frequencies,  $\bar{\nu}_{a_{1g}}$ , were obtained with accuracies of  $\pm 0.001 \text{ \AA}$  and  $\pm 1 \text{ cm}^{-1}$ , respectively (see Ref. 39 for additional details).

We also optimized the geometry of the  $(\text{LnCl}_6)^{3-}$  clusters using simpler representations of the  $\text{Cs}_2\text{NaYCl}_6$  host

TABLE I. Ln–Cl equilibrium distance of the  $\text{Cs}_2\text{NaYCl}_6:(\text{LnCl}_6)^{3-}$  defects as calculated at the CASSCF (without dynamic electron correlation) and CASPT2 (with dynamic electron correlation) levels using the quantum mechanical AIMP embedding potential of the  $\text{Cs}_2\text{NaYCl}_6$  host. Results of CASSCF geometry optimizations corresponding to *in vacuo* and Madelung embeddings are also included. The local distortions relative to the Y–Cl experimental or calculated distances are also tabulated. All numbers in Å.

	Equilibrium distance				Local distortion		
	CASSCF		CASPT2	AIMP	$R_e - 2.619^a$	$R_e - 2.579^b$	Ionic radii <sup>c</sup>
	<i>in vacuo</i>	Madelung					
Ce	2.952	2.866	2.739	2.682	0.063	0.103	0.142
Pr	2.934	2.869	2.728	2.666	0.047	0.087	0.121
Nd	2.918	2.853	2.718	2.656	0.037	0.077	0.103
Pm	2.901	2.836	2.708	2.642	0.023	0.063	0.087
Sm	2.881	2.818	2.696	2.631	0.012	0.052	0.072
Eu	2.862	2.804	2.692	2.630	0.011	0.051	0.058
Gd	2.841	2.780	2.672	2.609	−0.010	0.030	0.046
Tb	2.825	2.765	2.660	2.595	−0.024	0.016	0.031
Dy	2.811	2.751	2.650	2.584	−0.035	0.005	0.016
Ho	2.793	2.734	2.637	2.571	−0.048	−0.008	0.002
Er	2.791	2.733	2.634	2.567	−0.052	−0.012	−0.011
Tm	2.777	2.720	2.624	2.556	−0.063	−0.023	−0.023
Yb	2.761	2.703	2.611	2.544	−0.075	−0.035	−0.034
Lu	2.754	2.697	2.606	2.539	−0.080	−0.040	−0.044
Lu–Ce	−0.198	−0.169	−0.133	−0.143			

<sup>a</sup>CASPT2 values of  $R_e(\text{Ln–Cl})$  minus crystallographic value  $R(\text{Y–Cl}) = 2.619$  Å from Ref. 52.

<sup>b</sup>CASPT2 values of  $R_e(\text{Ln–Cl}) - R_e(\text{Y–Cl})$ .

<sup>c</sup>Difference of ionic radii [ $r(\text{Ln}^{3+}) - r(\text{Y}^{3+})$ ] from Refs. 41 and 42.

crystal in order to ascertain the effects of classical and quantum mechanical interactions between the  $(\text{LnCl}_6)^{3-}$  and the host crystal. We performed calculations, which will be referred to as *in vacuo* calculations, using the Hamiltonian of Eq. (1) after removing the whole AIMP embedding potential:

$$\hat{H}_{\text{spin-free}}^{\text{in vacuo}} = \hat{H}_{\text{spin-free}}^{\text{AIMP}} - \sum_{i=1}^{N_{\text{val}}^{\text{clus}}} \sum_{\xi \in \text{host}}^{N_{\text{ion}}^{\text{host}}} \hat{V}_{\xi-\text{ion}}^{\text{emb-AIMP}}(i).$$

We also performed calculations, which will be referred to as Madelung calculations, using the Hamiltonian of Eq. (1) excluding all the quantum mechanical terms of the AIMP embedding potential [Eq. (3)]:

$$\hat{H}_{\text{spin-free}}^{\text{Madelung}} = \hat{H}_{\text{spin-free}}^{\text{AIMP}} - \sum_{i=1}^{N_{\text{val}}^{\text{clus}}} \sum_{\xi \in \text{host}}^{N_{\text{ion}}^{\text{host}}} \left[ \hat{V}_{\xi-\text{ion}}^{\text{emb-AIMP}}(i) - \frac{Q_{\xi}}{r_{\xi i}} \right].$$

The results of the bond lengths,  $R_e$ , and totally symmetric vibrational frequencies,  $\bar{\nu}_{a_{1g}}$ , of the  $(\text{LnCl}_6)^{3-}$  embedded clusters are presented in Tables I and II, and Figs. 1–4, and are discussed next.

The host effects can be assessed and analyzed by comparing *in vacuo* with Madelung results (which shows the effects of a classical embedding), and Madelung with AIMP results (which shows the effects of quantum mechanical interactions between the cluster and its surroundings), at the CASSCF level described in Sec. II B. The effects of including dynamic electron correlation within the  $(\text{LnCl}_6)^{3-}$  cluster can be assessed by comparing the CASSCF and CASPT2 calculations which include the AIMP embedding.

Starting from the *in vacuo* results (see Table I and Fig. 1), the embedding effects are found to reduce the bond lengths considerably: The classical Madelung embedding po-

tential reduces the  $R_e$  values by 0.09–0.06 Å; the quantum mechanical interaction terms of the AIMP embedding further reduce the bond lengths by 0.13–0.09 Å, across the series. The intracluster electron correlation adds a final, but smaller reduction that amounts to 0.06–0.07 Å. The host effects on the lanthanide bond length contraction, illustrated by the variations of the  $R_e(\text{Lu}) - R_e(\text{Ce})$  values in Table I and Fig. 1, are found to be larger and of opposite sign than the intracluster electron correlation effects.

The results show that the local distortion produced by the  $\text{Ln}^{3+}$  impurities, measured as the difference between the Ln–Cl and Y–Cl bond lengths, is neither negligible, nor constant across the series. We have included the local distortions relative to the crystallographic value  $R(\text{Y–Cl}) = 2.619$  Å and the difference of ionic radii [ $r(\text{Ln}^{3+}) - r(\text{Y}^{3+})$ ] from Refs. 41 and 42 in Table I and Fig. 2 which show a different slope and a shift of around 0.04 Å. When we refer the local distortions to the  $R_e(\text{Y–Cl})$  2.579 Å value obtained in this work, instead, the comparison of their values and the estimations based on ionic radii reveals only a different slope across the series (Fig. 2). The difference in slope indicates that the lanthanide contraction derived from calculated bond lengths is smaller than that obtained from ionic radii. This result has already been found in previous *ab initio* studies of the lanthanide and actinide contraction in monohydride, monofluoride, and monooxide molecules in gas phase, and has been interpreted as due to the change in the bonding when proceeding from the first to the last element in the lanthanide series.<sup>43</sup>

The calculated bond distances can be used to discuss the assumptions usually made when the Judd–Morrison model is used for the analysis and predictions of  $4f \rightarrow 5d$  transitions



TABLE II. Totally symmetric vibrational frequency,  $\bar{\nu}_{a_{1g}}$ , of the  $\text{Cs}_2\text{NaYCl}_6:(\text{LnCl}_6)^{3-}$  defects as calculated at the CASSCF (without dynamic electron correlation) and CASPT2 (with dynamic electron correlation) levels using the quantum mechanical AIMP embedding potential of the  $\text{Cs}_2\text{NaYCl}_6$  host. CASSCF results corresponding to *in vacuo* and Madelung embeddings are also included. Experimental values corresponding to low temperature emission spectra of the  $\text{Cs}_2\text{NaYCl}_6:\text{Ln}^{3+}$  doped crystals (Refs. 17 and 19), and vibrational Raman (Refs. 44–48) and absorption and magnetic circular dichroism spectra (Refs. 50 and 51) for the  $\text{Cs}_2\text{NaLnCl}_6$  perfect crystals are also included. All numbers in  $\text{cm}^{-1}$ .

	Theoretical				Experiment				
	CASSCF			CASPT2 AIMP	$\text{Cs}_2\text{NaYCl}_6:\text{Ln}^{3+}$	$\text{Cs}_2\text{NaLnCl}_6$			
	<i>in vacuo</i>	Madelung	AIMP			References			
						48	44, 45	46, 47	50, 51
Ce	192	215	309	305	300 <sup>a</sup>		279	279	
Pr	193	216	308	306	298 <sup>b</sup>			282	
Nd	198	220	308	305		277 <sup>c</sup>	284.5	285	
Pm	200	223	308	304					
Sm	202	226	307	305			287	287	
Eu	207	232	313	313		302		290	
Gd	205	231	310	310				290	
Tb	206	232	308	309		298	292.5	292	302
Dy	205	232	306	310			295	295	
Ho	206	233	306	309			294	297	
Er	207	233	304	306		296	298	297	
Tm	208	234	303	305		295	296	297	302
Yb	206	233	302	306			299	296	
Lu	210	235	302	305					

<sup>a</sup>Reference 19.

<sup>b</sup>Reference 17.

<sup>c</sup>Reference 49.

in hosts doped with Ln ions. In effect, it is normally assumed that the bond distance between Ln and the ligands in a given host is independent of the Ln ion, so that the  $S$  factor,  $S = \sum_i \alpha_i Z_i e^2 / R_i^6$ , which involves an electronic dependence from the ligand (*via*  $\alpha_i$ ) and a structural dependence, becomes host-only dependent. Here we show that the variation of  $S$  across the whole lanthanide series in a given host can be as large as 39%. [In the present host,  $S(\text{Ln})/S(\text{Ce}) = (R_e(\text{Ce-Cl})/R_e(\text{Ln-Cl}))^6$ .] According to this, the observation that the depression of the  $5d$  level in a given host crystal,  $\Delta_{fd}^0 - \Delta_{fd} = \sigma_2 S$ , appears to be the same for all the  $\text{Ln}^{3+}$

ions within  $\pm 600 \text{ cm}^{-1}$  (Ref. 22) would indicate that the significant increase of  $S$  across the series is largely compensated by an also significant decrease of  $\sigma_2$ .

We can comment now on the results of the symmetric stretching mode vibrational frequency,  $\bar{\nu}_{a_{1g}}$ , for the ground state of the  $\text{Cs}_2\text{NaYCl}_6:(\text{LnCl}_6)^{3-}$  defects, which appear in Table II and Fig. 3. The most notable result is that the host effects on the vibrational frequencies are much larger than the intracluster effects of electron correlation (see Fig. 3) and they produce a notable increase of the vibrational frequen-

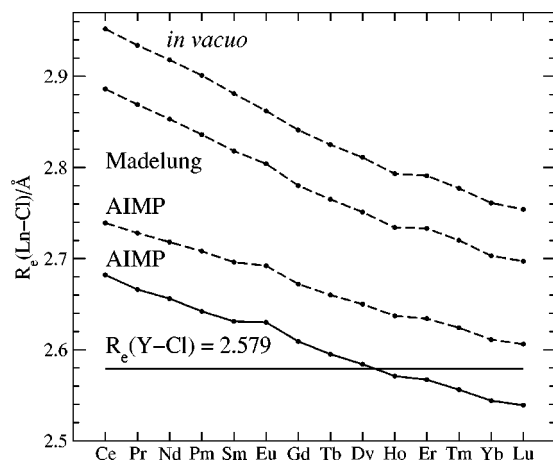


FIG. 1. Ln-Cl bond lengths of the  $\text{Cs}_2\text{NaYCl}_6:(\text{LnCl}_6)^{3-}$  defects as calculated at the CASSCF level (dashed lines) using *in vacuo*, Madelung, and AIMP embedding models. AIMP results for the  $\text{Cs}_2\text{NaYCl}_6:(\text{LnCl}_6)^{3-}$  series and for  $\text{Cs}_2\text{NaYCl}_6:(\text{YCl}_6)^{3-}$ , which incorporate electron correlation with the CASPT2 method, are also plotted (solid lines). All distances in Å.

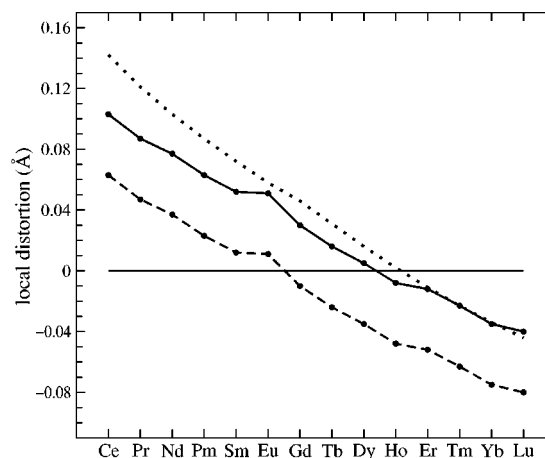


FIG. 2. Local distortions produced by the  $\text{Ln}^{3+}$  impurities in the  $\text{Cs}_2\text{NaYCl}_6$  host calculated as the difference in  $R_e(\text{Ln-Cl})$  and  $R_e(\text{Y-Cl})$  bond lengths using the AIMP embedding and the CASPT2 method (solid line), calculated relative to the crystallographic  $R(\text{Y-Cl}) = 2.619 \text{ Å}$  distance from Ref. 52 (dashed line), and estimated as the mismatch of ionic radii,  $r(\text{Ln}^{3+}) - r(\text{Y}^{3+})$ , from Refs. 41 and 42 (dotted line).

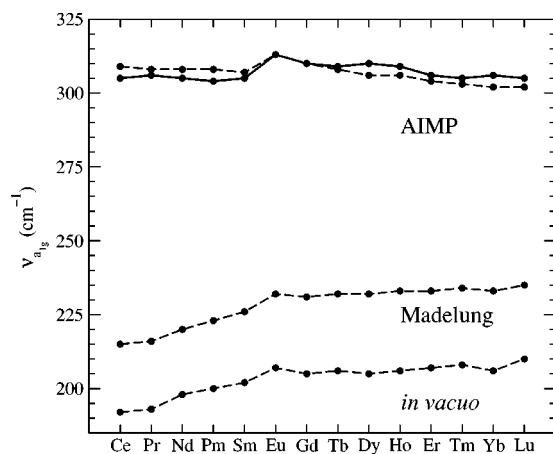


FIG. 3. Totally symmetric vibrational frequencies of the  $\text{Cs}_2\text{NaYCl}_6:(\text{LnCl}_6)^{3-}$  defects as calculated at the CASSCF level (dashed lines) using *in vacuo*, Madelung, and AIMP embedding models. AIMP results which incorporate electron correlation with the CASPT2 method, are also plotted (solid lines).

cies. It is also interesting to note that the quantum mechanical host effects are much larger than the classical Madelung effects and they are more pronounced going left in the series, from Lu to Ce. In effect, the classical Madelung embedding increases the vibrational frequencies by 23–25  $\text{cm}^{-1}$  from Ce to Lu, whereas the quantum mechanical terms add a further increase of some 94–67  $\text{cm}^{-1}$ . These observations can be related with the host effects on the bond lengths commented above. Altogether, the host effects on the bond lengths and vibrational frequencies and their variation across the series lead to the following conclusions: (i) host effects contribute strongly to strengthen the Ln–Cl bonding, since they produce shorter bond distances and higher vibrational frequencies of the symmetric bond stretching mode, (ii) the quantum mechanical terms of the embedding have more im-

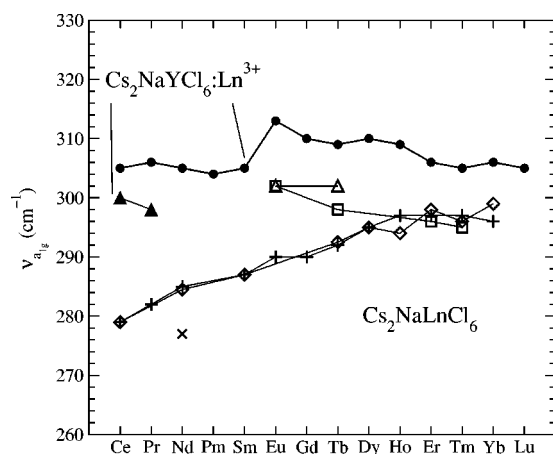


FIG. 4. Totally symmetric vibrational frequency,  $\bar{\nu}_{a_{1g}}$ , of the  $\text{Cs}_2\text{NaYCl}_6:(\text{LnCl}_6)^{3-}$  defects (full symbols) as calculated at the CASPT2 level using the quantum mechanical AIMP embedding potential of the  $\text{Cs}_2\text{NaYCl}_6$  host ( $\bullet$ ) and experimental values corresponding to low temperature emission spectra of the  $\text{Cs}_2\text{NaYCl}_6:\text{Ln}^{3+}$  doped crystals (full triangles; Refs. 17, 19). Vibrational Raman ( $\square$ , Ref. 48;  $\times$ , Ref. 49;  $\diamond$ , Ref. 44, 45;  $+$ , Ref. 46, 47) and absorption and magnetic circular dichroism spectra ( $\triangle$ , Refs. 50, 51) for the  $\text{Cs}_2\text{NaLnCl}_6$  perfect crystals are also included.

pact in the bonding than the Madelung terms, and (iii) the quantum mechanical interactions between the cluster and its surroundings are stronger going left in the series, from Lu to Ce, as it corresponds to the fact that the distance between the cluster ligands and the host ions becomes smaller.

Experimental data on the  $\bar{\nu}_{a_{1g}}$  vibrational frequencies of the ground electronic state of  $\text{Cs}_2\text{NaYCl}_6:\text{Ln}^{3+}$  crystals are only available for  $\text{Ce}^{3+}$  and  $\text{Pr}^{3+}$ , to our knowledge; their values have been extracted from the vibrational progressions of low temperature *d–f* emission spectra.<sup>17,19</sup> The agreement of our theoretical results with these values (see Table II and Fig. 4) is very satisfactory and points out the accuracy of the methods that have been used. Similar accuracies have been demonstrated on previous tests of theoretical vibrational frequencies versus experimental data on  $\text{Cs}_2\text{ZrCl}_6:\text{Pa}^{4+}$ .<sup>8</sup>

The remaining experimental values of vibrational frequencies do not correspond to doped crystals but to  $\text{Cs}_2\text{NaLnCl}_6$  perfect crystals. The comparison of the experimental data on  $\text{Ce}^{3+}$  (300  $\text{cm}^{-1}$ )<sup>19</sup> and  $\text{Pr}^{3+}$  (298  $\text{cm}^{-1}$ )<sup>17</sup> in  $\text{Cs}_2\text{NaYCl}_6$  with the perfect crystal values measured on  $\text{Cs}_2\text{NaCeCl}_6$  (279  $\text{cm}^{-1}$ )<sup>44–47</sup> and  $\text{Cs}_2\text{NaPrCl}_6$  (282  $\text{cm}^{-1}$ ),<sup>46,47</sup> respectively (Table II, Fig. 4), makes it reasonable to expect that the vibrational frequencies measured on the rest of  $\text{Cs}_2\text{NaLnCl}_6$  crystals should be smaller than those corresponding to the  $\text{Cs}_2\text{NaYCl}_6:\text{Ln}^{3+}$  defect crystals across the series. Considering this, the comparison of our doped crystal results with the  $\text{Cs}_2\text{NaLnCl}_6$  experiments should be meaningful, and, therefore, we have included available experimental data on  $\text{Cs}_2\text{NaLnCl}_6$  in Table II, and Fig. 4 for comparisons. The  $\text{Cs}_2\text{NaLnCl}_6$  experimental data produced by Haley and Koningstein,<sup>48</sup> Cheng and Dorain,<sup>49</sup> Amberger *et al.*,<sup>44,45</sup> and Tanner *et al.*,<sup>46,47</sup> correspond to low temperature vibrational Raman; those published by Schwartz *et al.*,<sup>50,51</sup> correspond to low temperature *f–f* absorption and magnetic circular dichroism spectra. Altogether, they show basically two different trends across the series (see Fig. 4): whereas the data from Amberger *et al.*,<sup>44,45</sup> and Tanner *et al.*<sup>46,47</sup> ( $\diamond$  and  $+$  in Fig. 4) show an increase of the  $\bar{\nu}_{a_{1g}}$  values from Ce to Lu, the results of Haley and Koningstein<sup>48</sup> ( $\square$  in Fig. 4) show decreasing values from Eu to Tm. Our results compare best with the latter: our  $\bar{\nu}_{a_{1g}}$  values appear to be higher (as they should be, according to what has been discussed above) and parallel (from Eu to Tm) to those of Haley and Koningstein.<sup>48</sup>

#### IV. CONCLUSIONS

In this paper we have studied two structural properties of  $\text{Ln}^{3+}$  impurities ( $\text{Ln}=\text{Ce}$  to  $\text{Lu}$ ) in the  $\text{Cs}_2\text{NaYCl}_6$  host crystal: the Ln–Cl bond length and the frequency of the  $(\text{LnCl}_6)^{3-}$  symmetric stretch. The model for the Ln–Cl interactions used takes into account relativistic effects through the use of Wood–Boring AIMP effective core potentials and bonding interactions, including 48 +  $n$  ( $n=1$  to 14) electron correlation, through the calculation of complete active space self-consistent-field (CASSCF) wave functions and energies followed by second order perturbation treatment (CASPT2). Interactions beyond first neighbors, between the  $(\text{LnCl}_6)^{3-}$  cluster and frozen Hartree–Fock wave functions representing

the external  $\text{Cs}^+$ ,  $\text{Na}^+$ ,  $\text{Y}^{3+}$ , and  $\text{Cl}^-$  host ions, were modeled by the AIMP embedding operators. Simpler (*in vacuo* and Madelung) representations of the embedding host were also considered in order to ascertain the contribution of separate cluster-lattice interaction terms of the AIMP embedded cluster Hamiltonian to the bonding properties and their variation across the lanthanide series. The analyses of the results show that host effects, particularly those of quantum mechanical nature, strongly contribute to strengthen the Ln–Cl bonds and that the Ln–Cl bonding properties are less sensitive to the host going right in the series from Ce to Lu. The intracluster electron correlation effects on the bond lengths are significant, reduce the bond distance values, and grow from Ce to Lu, whereas they are negligible on the frequencies of the symmetric bond stretching mode. Comparison between the calculated and available experimental values of the vibrational frequencies on the doped crystals  $\text{Cs}_2\text{NaYCl}_6:\text{Ce}^{3+}$  and  $\text{Cs}_2\text{NaYCl}_6:\text{Pr}^{3+}$  are very satisfactory. Their comparison with available experimental values on the neat  $\text{Cs}_2\text{NaLnCl}_6$  crystals, which show different variations going right in the series, is also presented and discussed. An important objective of this work, namely, the calculation of the Ln–Cl bond lengths in the  $\text{Cs}_2\text{NaYCl}_6:\text{Ln}^{3+}$  series, is an answer, from an independent, theoretical ground, to the concluding remarks of recent spectroscopists work.<sup>20</sup> The calculated bond distance values presented here should be useful to explicitly include the local distortions the  $\text{Ln}^{3+}$  produce in the  $\text{Cs}_2\text{NaYCl}_6$  host in the structural factor of the Judd–Morrison model for  $4f \rightarrow 5d$  transitions.

## ACKNOWLEDGMENTS

This work was partly supported by a grant from Ministerio de Ciencia y Tecnología, Spain (Dirección General de Investigación BQU2002-01316). B.O. acknowledges a fellowship (Beca FPI) from Ministerio de Ciencia y Tecnología, Spain.

- <sup>1</sup>S. Sugano, Y. Tanabe, and H. Kamimura, *Multiplets of Transition-Metal Ions in Crystal* (Academic, New York, 1970).
- <sup>2</sup>B. R. Judd, *Phys. Rev. Lett.* **39**, 242 (1977).
- <sup>3</sup>C. A. Morrison, *J. Chem. Phys.* **72**, 1001 (1980).
- <sup>4</sup>H. P. Andres, K. Krämer, and H. U. Güdel, *Phys. Rev. B* **54**, 3830 (1996).
- <sup>5</sup>Y. Shen and K. L. Bray, *Phys. Rev. B* **58**, 11944 (1998).
- <sup>6</sup>P. J. Dereń, W. Stręk, E. Zych, and J. Drożdżyński, *Chem. Phys. Lett.* **332**, 308 (2000).
- <sup>7</sup>N. M. Khaidukov, M. Kirm, S. K. Lam, D. Lo, V. N. Mkhov, and G. Zimmerer, *Opt. Commun.* **184**, 183 (2000).
- <sup>8</sup>L. Seijo and Z. Barandiarán, *J. Chem. Phys.* **115**, 5554 (2001).
- <sup>9</sup>L. Seijo and Z. Barandiarán, *J. Chem. Phys.* **118**, 5335 (2003).
- <sup>10</sup>Z. Barandiarán and L. Seijo, *J. Chem. Phys.* **118**, 7439 (2003).
- <sup>11</sup>L. Seijo, Z. Barandiarán, and B. Ordejón, *Mol. Phys.* **101**, 73 (2003).
- <sup>12</sup>Z. Barandiarán and L. Seijo, *J. Chem. Phys.* **119**, 3785 (2003).
- <sup>13</sup>J. P. Morley, T. R. Faulkner, F. S. Richardson, and R. W. Schwartz, *J. Chem. Phys.* **77**, 1734 (1982).
- <sup>14</sup>F. S. Richardson, M. F. Reid, J. J. Dallara, and R. D. Smith, *J. Chem. Phys.* **83**, 3813 (1985).
- <sup>15</sup>M. F. Reid and F. S. Richardson, *J. Chem. Phys.* **83**, 3831 (1985).
- <sup>16</sup>M. Laroche, M. Bettinelli, S. Girard, and R. Moncorgé, *Chem. Phys. Lett.* **311**, 167 (1999).
- <sup>17</sup>P. A. Tanner, C. S. K. Mak, and M. D. Faucher, *Chem. Phys. Lett.* **343**, 309 (2001).
- <sup>18</sup>P. A. Tanner, C. S. K. Mak, and M. D. Faucher, *J. Chem. Phys.* **114**, 10860 (2001).
- <sup>19</sup>P. A. Tanner, C. S. K. Mak, N. M. Edelstein, K. Murdoch, G. Liu, J. Huang, L. Seijo, and Z. Barandiarán (unpublished).
- <sup>20</sup>M. Bettinelli and R. Moncorgé, *J. Lumin.* **92**, 287 (2001).
- <sup>21</sup>P. Dorenbos, *J. Lumin.* **87–89**, 970 (2000).
- <sup>22</sup>P. Dorenbos, *J. Lumin.* **91**, 91 (2000).
- <sup>23</sup>Z. Barandiarán and L. Seijo, *J. Chem. Phys.* **89**, 5739 (1988).
- <sup>24</sup>L. Seijo and Z. Barandiarán, in *Computational Chemistry: Reviews of Current Trends*, edited by J. Leszczynski (World Scientific, Singapore, 1999), Vol. 4, p. 55.
- <sup>25</sup>S. Huzinaga, L. Seijo, Z. Barandiarán, and M. Klobukowski, *J. Chem. Phys.* **86**, 2132 (1987).
- <sup>26</sup>B. O. Roos, P. R. Taylor, and P. E. M. Siegbahn, *Chem. Phys.* **48**, 157 (1980); P. E. M. Siegbahn, A. Heiberg, J. Almlöf, and B. O. Roos, *J. Chem. Phys.* **74**, 2384 (1981); P. Siegbahn, A. Heiberg, B. Roos, and B. Levy, *Phys. Scr.* **21**, 323 (1980).
- <sup>27</sup>K. Andersson, P.-Å. Malmqvist, B. O. Roos, A. J. Sadlej, and K. Wolinski, *J. Phys. Chem.* **94**, 5483 (1990).
- <sup>28</sup>K. Andersson, P.-Å. Malmqvist, and B. O. Roos, *J. Chem. Phys.* **96**, 1218 (1992).
- <sup>29</sup>J. H. Wood and A. M. Boring, *Phys. Rev. B* **18**, 2701 (1978).
- <sup>30</sup>Z. Barandiarán and L. Seijo, *Can. J. Chem.* **70**, 409 (1992).
- <sup>31</sup>R. D. Cowan and D. C. Griffin, *J. Opt. Soc. Am.* **66**, 1010 (1976).
- <sup>32</sup>S. Huzinaga and A. A. Cantu, *J. Chem. Phys.* **55**, 5543 (1971).
- <sup>33</sup>Detailed core and embedding AIMP data libraries in electronic format are available from the authors upon request or directly at the address <http://www.uam.es/quimica/aimp/Data/AIMPLibs.html> (see also Ref. 40).
- <sup>34</sup>L. Seijo, Z. Barandiarán, and E. Harguindey, *J. Chem. Phys.* **114**, 118 (2001).
- <sup>35</sup>T. H. Dunning and P. J. Hay, in *Modern Theoretical Chemistry*, edited by H. F. Schaefer III (Plenum, New York, 1977).
- <sup>36</sup>J. Andzelm, M. Klobukowski, E. Radzio-Andzelm, Y. Sakai, and H. Tatewaki, in *Gaussian Basis Sets for Molecular Calculations*, edited by S. Huzinaga (Elsevier, Amsterdam, 1984).
- <sup>37</sup>A. Al-Abdalla, Z. Barandiarán, L. Seijo, and R. Lindh, *J. Chem. Phys.* **108**, 2005 (1998).
- <sup>38</sup>J. L. Pascual, L. Seijo, and Z. Barandiarán, *J. Chem. Phys.* **98**, 9715 (1993).
- <sup>39</sup>L. Seijo and Z. Barandiarán, *J. Chem. Phys.* **118**, 1921 (2003).
- <sup>40</sup>K. Andersson, M. Barysz, A. Bernhardsson *et al.*, MOLCAS version 5, Lund University, Sweden, 2000.
- <sup>41</sup>R. D. Shannon and C. T. Prewitt, *Acta Crystallogr., Sect. B: Struct. Crystallogr. Cryst. Chem.* **25**, 925 (1969).
- <sup>42</sup>R. D. Shannon, *Acta Crystallogr., Sect. A: Cryst. Phys., Diff., Theor. Gen. Crystallogr.* **32**, 751 (1976).
- <sup>43</sup>W. Küchle, M. Dolg, and H. Stoll, *J. Phys. Chem. A* **101**, 7128 (1997).
- <sup>44</sup>H. D. Amberger, G. G. Rosenbauer, and R. D. Fischer, *Mol. Phys.* **32**, 1291 (1976).
- <sup>45</sup>H. D. Amberger, G. G. Rosenbauer, and R. D. Fischer, *J. Phys. Chem. Solids* **38**, 379 (1977).
- <sup>46</sup>P. A. Tanner, X. Shangda, L. Yu-long, and M. Yi, *Phys. Rev. B* **55**, 12182 (1997).
- <sup>47</sup>L. Ning, P. A. Tanner, and X. Shangda, *Vib. Spectrosc.* **31**, 51 (2003).
- <sup>48</sup>L. V. Haley and J. A. Koningstein, *J. Raman Spectrosc.* **5**, 305 (1976).
- <sup>49</sup>C. Cheng and P. B. Dorain, *J. Chem. Phys.* **65**, 785 (1976).
- <sup>50</sup>R. W. Schwartz, H. G. Brittain, J. P. Riehl, W. Yeakel, and F. S. Richardson, *Mol. Phys.* **34**, 361 (1977).
- <sup>51</sup>R. W. Schwartz, T. R. Faulkner, and F. S. Richardson, *Mol. Phys.* **38**, 1767 (1979).
- <sup>52</sup>C. Reber, H. U. Güdel, G. Meyer, T. Schleid, and C. A. Daul, *Inorg. Chem.* **28**, 3249 (1989).